FITEE

Band-gap tunable $(Ga_xIn_{1-x})_2O_3$ layer grown by magnetron sputtering[*]

Fabi ZHANG[†1], Jinyu SUN[1], Haiou LI[1], Juan ZHOU[1], Rong WANG[1], Tangyou SUN[1],

Tao FU[1], Gongli XIAO[1], Qi LI[1], Xingpeng LIU[1], Xiuyun ZHANG[1],

Daoyou GUO[2], Xianghu WANG[3], Zujun QIN[†‡1]

[1]Guangxi Key Laboratory of Precision Navigation Technology and Application,

Guilin University of Electronic Technology, Guilin 541004, China

[2]Center for Optoelectronics Materials and Devices & Key Laboratory of Optical Field Manipulation of Zhejiang Province,

Zhejiang Sci-Tech University, Hangzhou 310018, China

[3]School of Mechanical Engineering, Shanghai Dianji University, Shanghai 200245, China

[†]E-mail: zhangfabi@outlook.com; qinzj@guet.edu.cn

Received July 8, 2020; Revision accepted Nov. 11, 2020; Crosschecked Sept. 2, 2021

Abstract: Multicomponent oxide $(Ga_xIn_{1-x})_2O_3$ films are prepared on (0001) sapphire substrates to realize a tunable band-gap by magnetron sputtering technology followed by thermal annealing. The optical properties and band structure evolution over the whole range of compositions in ternary compounds $(Ga_xIn_{1-x})_2O_3$ are investigated in detail. The X-ray diffraction spectra clearly indicate that $(Ga_xIn_{1-x})_2O_3$ films with Ga content varying from 0.11 to 0.55 have both cubic and monoclinic structures, and that for films with Ga content higher than 0.74, only the monoclinic structure appears. The transmittance of all films is greater than 86% in the visible range with sharp absorption edges and clear fringes. In addition, a blue shift of ultraviolet absorption edges from 380 to 250 nm is noted with increasing Ga content, indicating increasing band-gap energy from 3.61 to 4.64 eV. The experimental results lay a foundation for the application of transparent conductive compound $(Ga_xIn_{1-x})_2O_3$ thin films in photoelectric and photovoltaic industry, especially in display, light-emitting diode, and solar cell applications.

Key words: $(Ga_xIn_{1-x})_2O_3$ films; Band-gap tunable; Magnetron sputtering

https://doi.org/10.1631/FITEE.2000330　　　　　　　　　**CLC number:** TN304

1 Introduction

Indium oxide In_2O_3 is a wide band-gap (3.6 eV) transparent semiconductor with high infrared reflectance, conductivity, and transmittance to visible light (Veeraswamy et al., 2013; Manoharan et al., 2015; Reddy et al., 2017).

Indium oxide has been used in various optoelectronic devices, such as ultraviolet–blue light-emitting diodes (Chen ZM et al., 2017), laser diodes (Pourhashemi et al., 2015), thin-film phototransistors (Mottram et al., 2016), ultraviolet (UV) photodetectors (Chang et al., 2015b), and resonant tunneling devices (Labram et al., 2016). However, the band-gap of In_2O_3 needs to be enlarged to allow the

design of devices such as highly sensitive wavelength tunable photo-detectors and cutoff wavelength tunable optical filters. The band-gap of In_2O_3 can be enlarged by alloying with Ga_2O_3, which has a larger band-gap value (4.9 eV) than In_2O_3. Moreover, because of the similar orbital structure of Ga and In components, metal ion replacement can be expected for a smooth evolution of the optical band-gap (Schmidt-Grund et al., 2014). Compared with indium oxide, the defect of $(Ga_xIn_{1-x})_2O_3$ can be inhibited by the stronger Ga-O bonds (Lee HY et al., 2018). Band-gap modulation creates higher potential for the application of $(Ga_xIn_{1-x})_2O_3$ in UV optoelectronics (Yang et al., 2009). Because of its unique characteristics, this material has great potential for application in $(Ga_xIn_{1-x})_2O_3$-based photodetectors (Kranert et al., 2014), phase change memory devices (Ramzan et al., 2013), and so on.

Several methods have been used to grow a $(Ga_xIn_{1-x})_2O_3$ layer. Suzuki et al. (2014) fabricated α-$(Ga_xIn_{1-x})_2O_3$ by chemical vapor deposition (CVD), which enabled band-gap modulation from 5.3 to 4.0 eV with decreasing Ga content x from 0.95 to 0.33. Baldini et al. (2014) grew $(Ga_xIn_{1-x})_2O_3$ epitaxial layers by metal organic vapor phase epitaxy (MOVPE), and the variation of band-gap was confirmed from 4.89 to 4.98 eV with increasing Ga content from 0.91 to 0.98. Kokubun et al. (2010) prepared $(Ga_xIn_{1-x})_2O_3$ films using the sol-gel method, which showed a tunable band-gap from 5.0 to 4.2 eV. Prozheeva et al. (2018) discussed the relationship of alloy composition and the vacancy defect formation of deposited $(Ga_xIn_{1-x})_2O_3$ thin films by pulsed laser deposition (PLD). Zhang et al. (2014) confirmed band-gap tunable $(Ga_xIn_{1-x})_2O_3$ films by PLD, where the band-gap can be adjusted from 3.8 to 5.1 eV.

Magnetron sputtering is a low-cost standard technique and allows for good process control as well as reproducible batch processing (Abdullah et al., 2018). It can obtain high-quality films, and can be easily modified for industrial production (Reddy et al., 2017). Chang et al. (2015a) fabricated amorphous $(Ga_xIn_{1-x})_2O_3$ metal–semiconductor–metal UV photodetectors on glass by co-sputtering. They found that the cutoff wavelength of the modulated photodetectors could be modified by changing the radio-frequency (RF) sputtering power of the In_2O_3 target. Chen F et al. (2019) prepared amorphous gallium indium oxide thin-film transistors by co-sputtering, and found that the oxygen vacancies depend strongly on the indium content.

However, the grown $(Ga_xIn_{1-x})_2O_3$ films reported are all of amorphous structure and the Ga content range is limited. In this work, we grow crystalline $(Ga_xIn_{1-x})_2O_3$ films on a sapphire (0001) substrate by magnetron sputtering, and the Ga content x varies over a large range of 0.1–0.9. The structural and optical properties of the obtained films are investigated in detail.

2 Experimental details

$(Ga_xIn_{1-x})_2O_3$ layers were deposited on a sapphire (0001) substrate by a magnetron sputtering system at room temperature. Before growth, we washed the sapphire substrates with acetone, methanol, and deionized water, and dried them in blowing nitrogen. Then, they were chemically etched in a hot solution with the volume rate of H_2SO_4:H_3PO_4=3:1, rinsed in deionized water, and dried in nitrogen. Finally, the substrates were fixed in the vacuum chamber. The 99.99% purity bulk Ga_2O_3 and In_2O_3 (76.2 mm in diameter and 5 mm in thickness) were used as the sputtering targets. The deposition chamber was pumped down to a base pressure of 5.33×10^{-3} Pa by mechanical pumps and turbomolecular pumps. The flow rates of high-purity argon and oxygen (99.999%) were 600 and 150 standard cubic centimeters per minute, respectively. The gas flow rates were controlled using an MKS mass flow controller. Depositions were carried out at a pressure of 2.67×10^{-2} Pa and at a constant substrate temperature of 300 K. The RF power was 300 W and the distance between the target and the substrate holder was 120 mm. Then $(Ga_xIn_{1-x})_2O_3$ films were obtained using the layered deposition method; the In_2O_3 and Ga_2O_3 films were deposited layer by layer, followed by high temperature alloying. This deposition process was repeated 30 times. The stoichiometry of the films was changed by adjusting the thickness ratio of Ga_2O_3 to In_2O_3 layers. The thickness values of Ga_2O_3 and In_2O_3 layers for each cycle were 1 and 9, 3 and 7, 5 and 5, 7 and 3, 9 and 1 nm, respectively. To crystallize the films, the as-deposited samples were annealed at 1000 °C in an air environment for 120 min. A

schematic describing the process of film preparation is shown in Fig. 1. The physical pictures of the prepared films are shown in Fig. 2.

After growth, the thickness of $(Ga_xIn_{1-x})_2O_3$ films was measured by a surface step profile analyzer
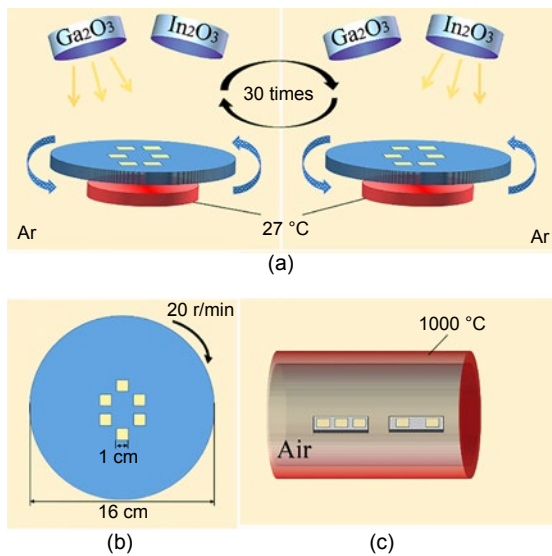

Fig. 1 Schematic of the film preparation process: (a) side view; (b) top view; (c) annealing processes
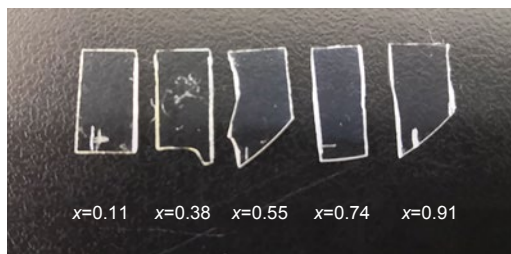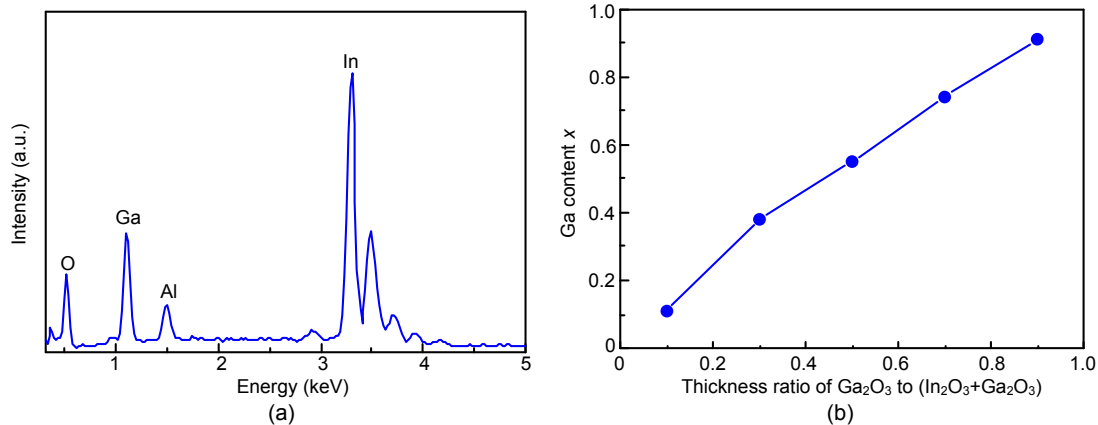

Fig. 2 Physical pictures of the prepared films

(Alpha-Step IQ, KLA-Tencore, USA). The composition of the films was measured by energy dispersive spectrometer (EDS) (X-Max20, Oxford, UK) within a scanning electron microscope (SEM) (Quanta FEG 450, FEI, USA). The crystal structure and crystal quality of the $(Ga_xIn_{1-x})_2O_3$ films were assessed by X-ray diffraction (XRD) (Empyrean Nano, PANalytical, the Netherlands). The surface morphology was examined by atomic force microscope (AFM) (MultiMode 8, Veecu/Broker, USA), and the root-mean-square (RMS) surface roughness R_q was estimated. In the wavelength range of 200–700 nm, the optical transmittance spectrum was recorded using a double-beam deep-UV spectroscope (UV3600, Shimadzu, Japan) with a deuterium lamp, and the bandgap E_g was estimated by analyzing the spectrum (Oshima et al., 2017).

3 Results and discussion

Representative EDS spectra of the films shown in Fig. 3a confirm that Ga, In, O, and Al elements were all prepared in the films, and the Ga content x as a function of the thickness ratio of Ga_2O_3 to $(In_2O_3+ Ca_2O_3)$ is given in Fig. 3b. The appearance peak of Al is caused by the sapphire substrate. No other elements appear, indicating high purity of the as-deposited films. The Ga content x increases almost linearly with the increase of the thickness ratio of Ga_2O_3 to $(In_2O_3+ Ga_2O_3)$. The Ga content x for films with the thickness ratio of 0.1, 0.3, 0.5, 0.7, and 0.9 is about 0.11, 0.38, 0.55, 0.74, and 0.91, respectively.

Fig. 3 Typical energy dispersive spectrometer spectrum of $(Ga_xIn_{1-x})_2O_3$ films (a) and Ga content x as a function of the thickness ratio of Ga_2O_3 to $(In_2O_3+Ca_2O_3)$ (b)

To investigate the effect of Ga content x on the crystal structure, XRD patterns of the $(Ga_xIn_{1-x})_2O_3$ films are shown in Fig. 4a. Along with the (006) peak from the sapphire substrate, the (222), (400), and (422) planes of cubic phase c-$(Ga_xIn_{1-x})_2O_3$ are distributed as peaks located at 30.7°, 35.6°, and 44.2°, respectively, according to the Joint Committee on Powder Diffraction Standards (JCPDS-06-0416). Diffraction peaks from the (−402), (−601), and (403) planes of monoclinic β-$(Ga_xIn_{1-x})_2O_3$ are located at 38.2°, 44.3°, and 64.5°, respectively, according to the standard cards (JCPDS-43043-1012). It is clear that for films
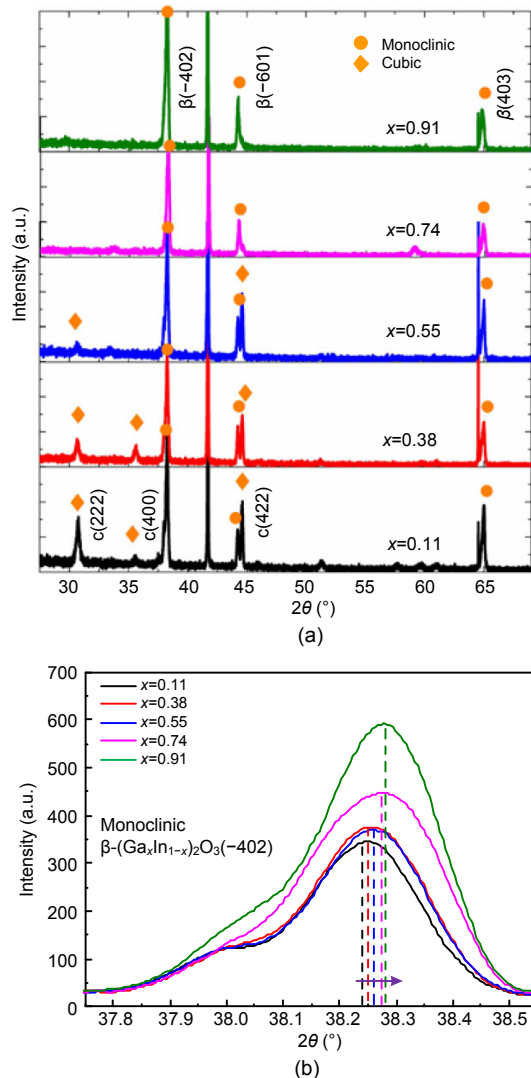
with Ga content x from 0.11 to 0.55, both cubic and monoclinic structures exist. For films with Ga content x higher than 0.74, only the monoclinic structure appears. von Wenckstern (2019) investigated $(Ga_xIn_{1-x})_2O_3$ alloys, finding that the solubility of Ga_2O_3 in cubic In_2O_3 was much lower than that of In_2O_3 in monoclinic Ga_2O_3, and that the solubility reached 75%. According to first-principle calculations, Maccioni et al. (2016) investigated Ga-doped cubic In_2O_3, finding that the solubility of Ga in In_2O_3 was less than 15%. Hassa et al. (2019) investigated In-doped monoclinic Ga_2O_3, and found that the solubility of In in monoclinic Ga_2O_3 was about 35%. Peelaers et al. (2015) investigated the electronic and structural properties of $(Ga_xIn_{1-x})_2O_3$ alloys. The solubility limit of In in β-Ga_2O_3 was 50%. Our results agree well with these conclusions mentioned above, indicating that our growth is of a thermal equilibrium condition.

Fig. 4b shows the enlarged (−402) peak of β-$(Ga_xIn_{1-x})_2O_3$. The (−402) peak shifts slightly towards higher angles with the increase in x (Priya et al., 2017). Given the smaller radius of Ga^{3+} (0.062 nm) compared with that of In^{3+} (0.081 nm), the systematic displacement of 2θ/θ scanning peaks implies that In ions are captured by Ga^{3+} sites in the Ga_2O_3 lattice (Jiang et al., 2011).

Fig. 5 depicts the $(Ga_xIn_{1-x})_2O_3$ film surfaces for different Ga content values. It can be seen that the surfaces of films are composed of dense and uniform grains, indicating good surface quality of these films (Jothibas et al., 2014; Demin and Kozlov, 2017), and that the grains are spherically shaped with diameters of approximately 30−60 nm. Fig. 6 summarizes the RMS roughness of the films based on the 4 μm×4 μm scanning area. The RMS roughness values for all films are below 5 nm, indicating smooth surfaces.

The optical nature and band-gap energy of the films were measured by UV–visible spectroscopy transmittance spectral analysis. The room-temperature optical transmittance spectra for the $(Ga_xIn_{1-x})_2O_3$ films are shown in Fig. 7a. The presence of interference fringes indicates good thickness uniformity and surface homogeneity (Beji et al., 2016). The transmittance of all films is higher than 86% in the visible range. Slight changes in the transparency of films are caused by surface roughness and incident light scattering (Wang et al., 2016). The sharp absorption edges
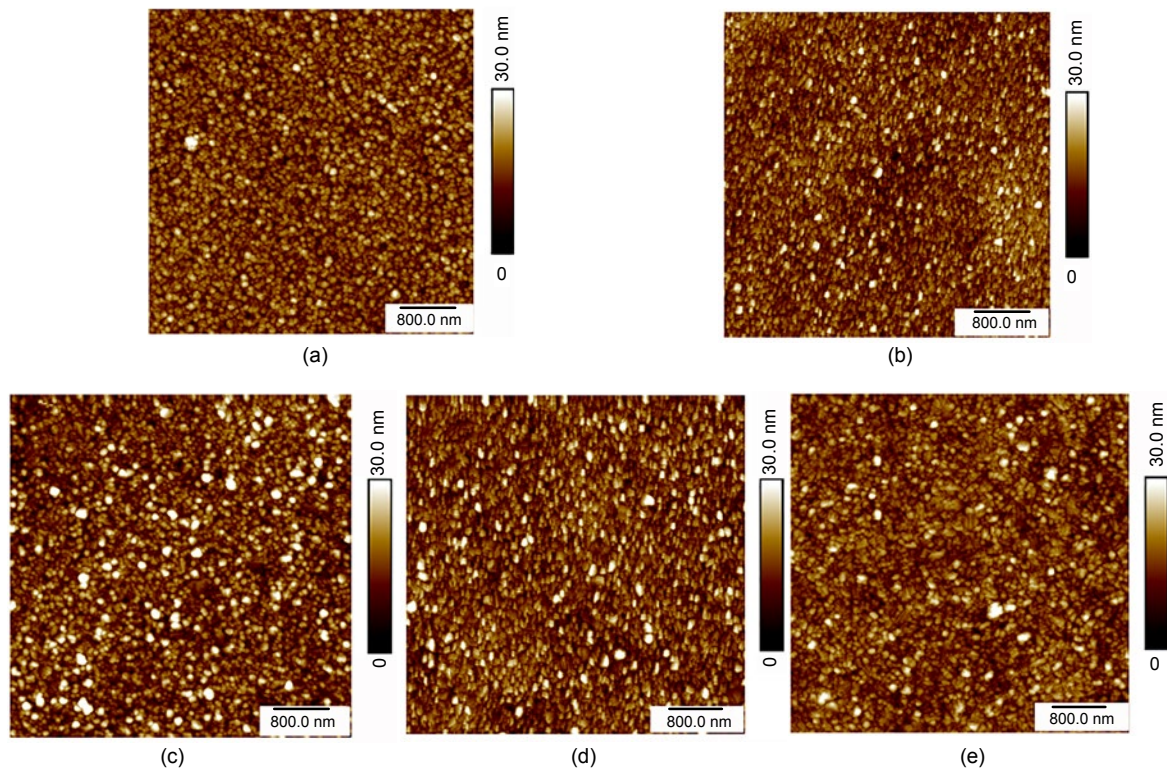

Fig. 4 X-ray diffraction (XRD) spectra of $(Ga_xIn_{1-x})_2O_3$ films at different Ga content values (a) and enlarged XRD pattern of the monoclinic (−402) peak in the films (b). References to color refer to the online version of this figure

Fig. 5　Surface atomic force microscope morphology of $(Ga_xIn_{1-x})_2O_3$ thin films with different Ga content values of x=0.11 (a), x=0.38 (b), x=0.55 (c), x=0.74 (d), and x=0.91 (e)

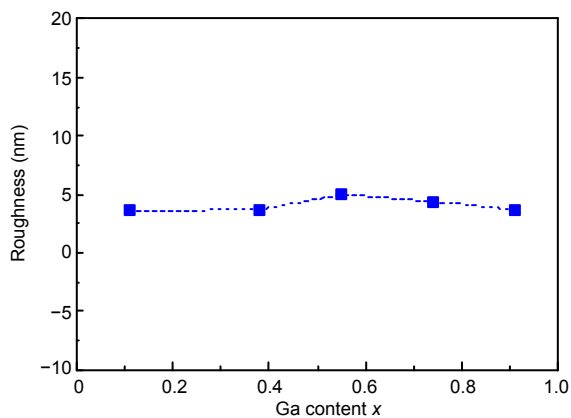**Fig. 6　Root-mean-square roughness of $(Ga_xIn_{1-x})_2O_3$ thin films with different Ga content values**

shifted towards shorter wavelengths from 380 to 250 nm with the increase in Ga content from 0.11 to 0.91.

Fig. 7b shows the dependence of $(\alpha h\upsilon)^2$ on $h\upsilon$ of $(Ga_xIn_{1-x})_2O_3$ films. In semiconductors, the energy requirement of the electronic transition between the valence band and the conduction band represents band-gap. The optical band-gap of the $(Ga_xIn_{1-x})_2O_3$ films can be analyzed by the following relationship

(Tauc and Menth, 1972; Senthilkumar and Vickraman, 2010; Hsu et al., 2015; Beji et al., 2016):

$$(\alpha h\upsilon)=A(h\upsilon-E_g)^n, \tag{1}$$

where A is the energy-independent constant, α the absorption coefficient, $h\upsilon$ the photon energy, and n=1/2 (Cabello et al., 2008; Jothibas et al., 2014). E_g values of the films are determined by extrapolating the line of $(\alpha h\upsilon)^2$ vs. $h\upsilon$ to $(\alpha h\upsilon)^2$=0 (Yakuphanoglu et al., 2015). The absorption coefficient α can be obtained by $\alpha=-(\ln T)/d$ (Mathen et al., 2017; Premkumar and Vadivel, 2017), where T and d are the optical transmittance and the thickness of $(Ga_xIn_{1-x})_2O_3$ films, respectively.

The band-gaps of films with different Ga content values are shown in Fig. 7c. For comparison, the reported band-gap values in Kokubun et al. (2010), Suzuki et al. (2014), and Chang et al. (2015a) were also provided. The band-gap values for films with Ga content values of 0.11, 0.38, 0.55, 0.74, and 0.91 were about 3.61, 3.74, 3.99, 4.25, and 4.64 eV, respectively. The band-gap values increased with the increase in Ga content, and the obtained band-gap values were in

agreement with those in the literature. The results indicated that the band-gap of $(Ga_xIn_{1-x})_2O_3$ can be controlled by increasing Ga content. In addition, the band-gap of the alloy is traditionally assumed to be related to the content (Wright and Nelson, 1995), $E_g(x)=f(x)-bx(1-x)$, where bowing parameter b is the

measurement of how far the band-gap of the alloy deviates from the linear interpolation between the pure phases (Lee SR et al., 1999). The band-gap energy of $(Ga_xIn_{1-x})_2O_3$ is correlated with the Ga content x according to the following (Chen KY et al., 2019):

$$E_g(x) = xE_{g(Ga_2O_3)} + (1-x)E_{g(In_2O_3)} - bx(1-x), \quad (2)$$

where $E_{g(In_2O_3)}$ and $E_{g(Ga_2O_3)}$ are the band-gap values of In_2O_3 and Ga_2O_3, respectively.

The band-gap results of $(Ga_xIn_{1-x})_2O_3$ are shown in Fig. 7c, and substituting these results into Eq. (2), a band-gap bowing parameter of (1.225 ± 0.221) eV was obtained. Kokubun et al. (2010) have shown that the band-gap decreases from 5.0 to 4.2 eV linearly as the Ga content decreases from 1.0 to 0.7. The results of von Wenckstern et al. (2015) and Suzuki et al. (2014) had the similar trend. Moreover, Peelaers et al. (2015) observed that $(Ga_xIn_{1-x})_2O_3$ alloy band-gap is close to its linearly interpolated value in the monoclinic structure, but the cubic structure band-gap bows with a bowing parameter b of 1.69 eV. There are various kinds of interfering factors on the bowing parameter b. Bellaiche et al. (1999) found that the bowing parameter b depends strongly on the composition. Kang et al. (2013) found that band bowing is a common effect of volume deformation, chemical difference, and low-dimensionality enhanced structure relaxation. The deviation of the bowing parameter b in this work compared with others should be related to the crystal structure and/or the grain size. Further investigation is needed to find out the mechanism.

It should also be noted that, as shown in Fig. 7a, both cubic crystal and monoclinic crystal structures existed in the films with Ga content of 0.11−0.55, but all the films showed a single transmittance. The single absorption edge should be related to the layered structure of deposition. The films were deposited layer-by-layer from Ga_2O_3 and In_2O_3 films. It is suggested that for films with Ga content lower than 0.11, Ga_2O_3 layer has diffused in In_2O_3 layer and formed c-$(Ga_xIn_{1-x})_2O_3$. For films with Ga content higher than 0.55, In_2O_3 layer has diffused in Ga_2O_3 layer and formed β-$(Ga_xIn_{1-x})_2O_3$. For films with Ga content between 0.11 and 0.55, after annealing process, both β-$(Ga_xIn_{1-x})_2O_3$ and c-$(Ga_xIn_{1-x})_2O_3$ are preserved. The absorption edge is determined by the layer with the smaller band-gap, i.e., the

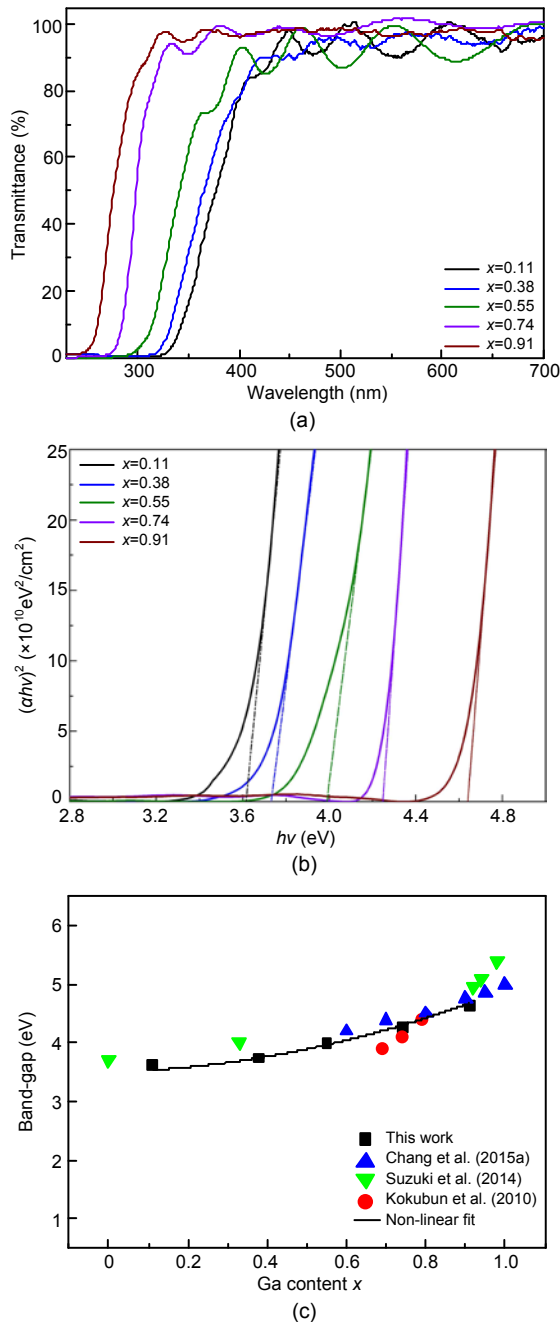**Fig. 7 Spectra of the transmittance for $(Ga_xIn_{1-x})_2O_3$ films (a), band-gap values calculated by extrapolating linear portions of $(\alpha h\upsilon)^2$ vs. $(h\upsilon)$ (b), and band-gap E_g of $(Ga_xIn_{1-x})_2O_3$ thin films (c). References to color refer to the online version of this figure**

c-$(Ga_xIn_{1-x})_2O_3$ layer (Zhang et al., 2019). Thus, only one absorption edge has been observed from the transmittance spectra.

4 Conclusions

In summary, transparent $(Ga_xIn_{1-x})_2O_3$ films with different Ga content values on sapphire (0001) substrates were grown by magnetron sputtering using Ga_2O_3 and In_2O_3 ceramic targets, with Ar and O_2 as reaction gases. For films with Ga content x from 0.11 to 0.55, both cubic and monoclinic structures existed, and for films with Ga content x higher than 0.74, only monoclinic structure appeared. The surfaces of films were dense and had uniform grains, with a good surface quality. All the films showed high transmittance in the visible range with sharp absorption edges. The band-gap energy increased from 3.61 to 4.64 eV with increasing Ga content x from 0.11 to 0.91. The above results suggested that magnetron sputtering is a promising growth technology for growth of band-gap tunable $(Ga_xIn_{1-x})_2O_3$ films. These films have been developed to design wavelength tunable photodetector and cutoff wavelength tuning optical filter.

Contributors

Fabi ZHANG and Zujun QIN designed the research. Jinyu SUN, Haiou LI, Juan ZHOU, and Rong WANG prepared the samples. Tangyou SUN, Tao FU, Gongli XIAO, Qi LI, Xingpeng LIU, and Xiuyun ZHANG measured the samples. Fabi ZHANG and Jinyu SUN drafted the manuscript. Daoyou GUO and Xianghu WANG helped organize the manuscript. Fabi ZHANG, Jinyu SUN, and Zujun QIN revised and finalized the paper.

Compliance with ethics guidelines

Fabi ZHANG, Jinyu SUN, Haiou LI, Juan ZHOU, Rong WANG, Tangyou SUN, Tao FU, Gongli XIAO, Qi LI, Xingpeng LIU, Xiuyun ZHANG, Daoyou GUO, Xianghu WANG, and Zujun QIN declare that they have no conflict of interest.

References

Abdullah SA, Sahdan MZ, Nafarizal N, et al., 2018. Influence of substrate annealing on inducing Ti^{3+} and oxygen vacancy in TiO_2 thin films deposited via RF magnetron sputtering. *Appl Surf Sci*, 462:575-582. https://doi.org/10.1016/j.apsusc.2018.08.137

Baldini M, Gogova D, Irmscher K, et al., 2014. Heteroepitaxy of $Ga_{2(1-x)}In_{2x}O_3$ layers by MOVPE with two different oxygen sources. *Cryst Res Technol*, 49(8):552-557. https://doi.org/10.1002/crat.201300410

Beji N, Souli M, Reghima M, et al., 2016. Study on the physical properties of europium doped indium oxide thin films. *Mater Sci Semicond Process*, 56:20-28. https://doi.org/10.1016/j.mssp.2016.07.013

Bellaiche L, Mattila T, Wang LW, et al., 1999. Resonant hole localization and anomalous optical bowing in InGaN alloys. *Appl Phys Lett*, 74:1842. https://doi.org/10.1063/1.123687

Cabello G, Lillo L, Caro C, et al., 2008. Structure and optical characterization of photochemically prepared ZrO_2 thin films doped with erbium and europium. *J Non-Cryst Sol*, 354(33):3919-3928. https://doi.org/10.1016/j.jnoncrysol.2008.05.029

Chang TH, Chang SJ, Chiu CJ, et al., 2015a. Bandgap-engineered in indium-gallium-oxide ultraviolet phototransistors. *IEEE Photon Technol Lett*, 27(8): 915-918. https://doi.org/10.1109/LPT.2015.2400446

Chang TH, Chang SJ, Weng WY, et al., 2015b. Amorphous indium–gallium–oxide UV photodetectors. *IEEE Photon Technol Lett*, 27(19):2083-2086. https://doi.org/10.1109/lpt.2015.2453317

Chen F, Ding S, Su WT, 2019. The synthesis and tunable optical properties of two-dimensional alloyed $Mo_{1-x}W_xS_2$ monolayer with in-plane composition modulations ($0 \leq x \leq 1$). *J Alloys Compd*, 784:213-219. https://doi.org/10.1016/j.jallcom.2019.01.049

Chen KY, Yang CC, Su YK, et al., 2019. Impact of oxygen vacancy on the photo-electrical properties of In_2O_3-based thin-film transistor by doping Ga. *Materials*, 12(5):737. https://doi.org/10.3390/ma12050737

Chen ZM, Zhuo Y, Tu WB, et al., 2017. Highly ultraviolet transparent textured indium tin oxide thin films and the application in light emitting diodes. *Appl Phys Lett*, 110(24):242101. https://doi.org/10.1063/1.4986452

Demin IE, Kozlov AG, 2017. Effect of composition on properties of In_2O_3–Ga_2O_3 thin films. *J Phys Conf Ser*, 858:012009. https://doi.org/10.1088/1742-6596/858/1/012009

Hassa A, von Wenckstern H, Splith D, et al., 2019. Structural, optical, and electrical properties of orthorhombic κ-$(In_xGa_{1-x})_2O_3$ thin films. *APL Mater*, 7(2):022525. https://doi.org/10.1063/1.5054394

Hsu CM, Tzou WC, Yang CF, et al., 2015. Investigation of the high mobility IGZO thin films by using co-sputtering method. *Materials*, 8(5):2769-2781. https://doi.org/10.3390/ma8052769

Jiang FX, Xu XH, Zhang J, et al., 2011. Room temperature ferromagnetism in metallic and insulating $(In_{1-x}Fe_x)_2O_3$ thin films. *J Appl Phys*, 109(5):053907. https://doi.org/10.1063/1.3559298

Jothibas M, Manoharan C, Ramalingam S, et al., 2014. Spectroscopic analysis, structural, microstructural, optical and electrical properties of Zn-doped In_2O_3 thin films. *Spectrochim Acta A Mol Biomol Spectrosc*, 122:

171-178. https://doi.org/10.1016/j.saa.2013.11.008

Kang J, Tongay S, Li JB, et al., 2013. Monolayer semiconducting transition metal dichalcogenide alloys: stability and band bowing. *J Appl Phys*, 113(14):143703. https://doi.org/10.1063/1.4799126

Kokubun Y, Abe T, Nakagomi S, 2010. Sol-gel prepared $(Ga_{1-x}In_x)_2O_3$ thin films for solar-blind ultraviolet photodetectors. *Phys Stat Sol A Appl Mater Sci*, 207(7): 1741-1745. https://doi.org/10.1002/pssa.200983712

Kranert C, Lenzner J, Jenderka M, et al., 2014. Lattice parameters and Raman-active phonon modes of $(In_xGa_{1-x})_2O_3$ for $x < 0.4$. *J Appl Phys*, 116(1):013505. https://doi.org/10.1063/1.4886895

Labram JG, Treat ND, Lin YH, et al., 2016. Energy quantization in solution-processed layers of indium oxide and their application in resonant tunneling diodes. *Adv Funct Mater*, 26(10):1656-1663. https://doi.org/10.1002/adfm.201503732

Lee HY, Liu JT, Lee CT, 2018. Modulated Al_2O_3-alloyed Ga_2O_3 materials and deep ultraviolet photodetectors. *IEEE Photon Technol Lett*, 30(6):549-552. https://doi.org/10.1109/lpt.2018.2803763

Lee SR, Wright AF, Crawford MH, et al., 1999. The band-gap bowing of $Al_xGa_{1-x}N$ alloys. *Appl Phys Lett*, 74(22):3344. https://doi.org/10.1063/1.123339

Maccioni MB, Ricci F, Fiorentini V, 2016. Properties of $(Ga_{1-x}In_x)_2O_3$ over the whole x range. *J Phys Condens Matt*, 28(22):224001. https://doi.org/10.1088/0953-8984/28/22/224001

Manoharan C, Jothibas M, Jeyakumar J, et al., 2015. Structural, optical and electrical properties of Zr-doped In_2O_3 thin films. *Spectrochim Acta A Mol Biomol Spectrosc*, 145: 47-53. https://doi.org/10.1016/j.saa.2015.02.099

Mathen JJ, Madhavan J, Thomas A, et al., 2017. Transparent ZnO–PVA binary composite for UV-A photo detector: optical, electrical and thermal properties followed by laser induced fluorescence. *J Mater Sci Mater Electron*, 28(10):7190-7203. https://doi.org/10.1007/s10854-017-6400-1

Mottram DA, Lin YH, Pattanasattayavong P, et al., 2016. Quasi two-dimensional dye-sensitized In_2O_3 phototransistors for ultrahigh responsivity and photosensitivity photodetector applications. *ACS Appl Mater Interf*, 8(7):4894-4902. https://doi.org/10.1021/acsami.5b11210

Oshima T, Kato Y, Oda M, et al., 2017. Epitaxial growth of γ-$(Al_xGa_{1-x})_2O_3$ alloy films for band-gap engineering. *Appl Phys Expr*, 10(5):051104. https://doi.org/10.7567/apex.10.051104

Peelaers H, Steiauf D, Varley JB, et al., 2015. $(In_xGa_{1-x})_2O_3$ alloys for transparent electronics. *Phys Rev B Cover Condens Matt Mater Phys*, 92(8):085206. https://doi.org/10.1103/PhysRevB.92.085206

Pourhashemi A, Farrell RM, Cohen DA, et al., 2015. High-power blue laser diodes with indium tin oxide cladding on semipolar ($20\bar{2}\bar{1}$) GaN substrates. *Appl Phys Lett*,

106(11):111105. https://doi.org/10.1063/1.4915324

Premkumar M, Vadivel S, 2017. Effect of annealing temperature on structural, optical and humidity sensing properties of indium tin oxide (ITO) thin films. *J Mater Sci Mater Electron*, 28(12):8460-8466. https://doi.org/10.1007/s10854-017-6566-6

Priya BS, Shanthi M, Manoharan C, et al., 2017. Hydrothermal synthesis of Ga-doped In_2O_3 nanostructure and its structural, optical and photocatalytic properties. *Mater Sci Semicond Process*, 71:357-365. https://doi.org/10.1016/j.mssp.2017.08.025

Prozheeva V, Hölldobler R, von Wenckstern H, et al., 2018. Effects of alloy composition and Si-doping on vacancy defect formation in $(In_xGa_{1-x})_2O_3$ thin films. *J Appl Phys*, 123(12):125705. https://doi.org/10.1063/1.5022245

Ramzan M, Kaewmaraya T, Ahuja R, 2013. Molecular dynamics study of amorphous Ga-doped In_2O_3: a promising material for phase change memory devices. *Appl Phys Lett*, 103(7):072113. https://doi.org/10.1063/1.4818788

Reddy IN, Reddy CV, Cho M, et al., 2017. Structural, optical and XPS study of thermal evaporated In_2O_3 thin films. *Mater Res Expr*, 4(8):086406. https://doi.org/10.1088/2053-1591/aa7f59

Schmidt-Grund R, Kranert C, Böntgen T, et al., 2014. Dielectric function in the NIR-VUV spectral range of $(In_xGa_{1-x})_2O_3$ thin films. *J Appl Phys*, 116(5):053510. https://doi.org/10.1063/1.4891521

Senthilkumar V, Vickraman P, 2010. Annealing temperature dependent on structural, optical and electrical properties of indium oxide thin films deposited by electron beam evaporation method. *Curr Appl Phys*, 10(3):880-885. https://doi.org/10.1016/j.cap.2009.10.014

Suzuki N, Kaneko K, Fujita S, 2014. Growth of corundum-structured $(In_xGa_{1-x})_2O_3$ alloy thin films on sapphire substrates with buffer layers. *J Cryst Growth*, 401:670-672. https://doi.org/10.1016/j.jcrysgro.2014.02.051

Tauc J, Menth A, 1972. States in the gap. *J Non-Cryst Sol*, 8-10: 569-585. https://doi.org/10.1016/0022-3093(72)90194-9

Veeraswamy Y, Vijayakumr Y, Reddy MV, et al., 2013. Structural and optical characterization of indium oxide thin films by vacuum thermal evaporation. Int Conf on Advanced Nanomaterials & Emerging Engineering Technologies, p.502-505. https://doi.org/10.1109/ICANMEET.2013.6609348

von Wenckstern H, 2019. 6-properties of $(In, Ga)_2O_3$ alloys. In: Pearton S, Ren F, Mastro M (Eds.), Gallium Oxide. Elsevier, Amsterdam, p.119-148. https://doi.org/10.1016/B978-0-12-814521-0.00006-3

von Wenckstern H, Splith D, Purfürst M, et al., 2015. Structural and optical properties of $(In, Ga)_2O_3$ thin films and characteristics of Schottky contacts thereon. *Semicond Sci Technol*, 30(2):024005. https://doi.org/10.1088/0268-1242/30/2/024005

Wang X, Chen ZW, Zhang FB, et al., 2016. Influence of substrate temperature on the properties of $(AlGa)_2O_3$ thin

films prepared by pulsed laser deposition. *Ceram Int*, 42(11):12783-12788. https://doi.org/10.1016/j.ceramint.2016.05.039

Wright AF, Nelson JS, 1995. Bowing parameters for zinc-blende $Al_{1-x}Ga_xN$ and $Ga_{1-x}In_xN$. *Appl Phys Lett*, 66(22): 3051. https://doi.org/10.1063/1.114274

Yakuphanoglu F, Gunduz B, Al-Ghamdi AA, et al., 2015. Transparent ultraviolet photodiodes based conductive gallium-indium-oxide films/p-type silicon for solar panel tracking systems. *Sens Actuat A Phys*, 234:212-222. https://doi.org/10.1016/j.sna.2015.09.010

Yang F, Ma J, Luan C, et al., 2009. Structural and optical properties of $Ga_{2(1-x)}In_{2x}O_3$ films prepared on α-Al_2O_3 (0001) by MOCVD. *Appl Surf Sci*, 255(8):4401-4404. https://doi.org/10.1016/j.apsusc.2008.10.129

Zhang FB, Saito K, Tanaka T, et al., 2014. Wide bandgap engineering of $(GaIn)_2O_3$ films. *Sol State Commun*, 186:28-31. https://doi.org/10.1016/j.ssc.2014.01.024

Zhang FB, Sun JY, Li HO, et al., 2019. Mixed phase $(GaIn)_2O_3$ films with a single absorption edge grown by magnetron sputtering. *J Electron Mater*, 48(12):8061-8066. https://doi.org/10.1007/s11664-019-07645-1